


Photoluminescence related to Ca in GaN

M. A. Reshchikov¹, D. O. Demchenko¹, M. Vorobiov¹, O. Andrieiev¹, B. McEwen², F. Shahedipour-Sandvik², K. Sierakowski³, A. Jaroszynska³, and M. Bockowski³

¹*Department of Physics, Virginia Commonwealth University, Richmond, Virginia 23220, USA*

²*College of Nanoscale Science and Engineering, SUNY Polytechnic Institute, Albany, New York 12203, USA*

³*Institute of High Pressure Physics, Polish Academy of Sciences, Sokolowska 29/37, Warsaw 01-142, Poland*

 (Received 14 April 2022; revised 28 June 2022; accepted 14 July 2022; published 28 July 2022)

The Ca_{Ga} acceptor in GaN was studied using photoluminescence (PL) experiments and first-principles calculations. The experimentally found $-/0$ transition level of the Ca_{Ga} at 0.50 ± 0.02 eV above the valence band reasonably agrees with the value calculated using the Heyd-Scuseria-Ernzerhof functional tuned to fulfill the generalized Koopmans condition (0.70 eV). The Ca_{Ga} acceptor is responsible for the green luminescence band (labeled GL_{Ca}) with a maximum at 2.5 eV. The electron- and hole-capture coefficients for the Ca_{Ga} acceptor are obtained from PL experiments: $C_n = 9 \times 10^{-14}$ cm³/s and $C_p = 6 \times 10^{-7}$ cm³/s. The GL_{Ca} band is an efficient radiative recombination channel in GaN samples implanted with Ca and in unintentionally doped GaN grown by molecular-beam epitaxy at relatively low temperatures, where Ca is a common contaminant.

DOI: [10.1103/PhysRevB.106.035206](https://doi.org/10.1103/PhysRevB.106.035206)

I. INTRODUCTION

GaN and its alloys with InN and AlN are important semiconductors used in numerous optical and electronic devices, including solid-state lighting and high-power electronics applications [1]. Point defects in GaN remain a limiting factor in the stability of devices and achieving high breakdown voltages. Photoluminescence (PL) is a powerful tool for studying point defects in semiconductors. While several defect-related PL bands in GaN are reliably identified, many questions remain [2,3].

Identifying point defects in GaN and determining their parameters is essential not only for technological progress but also for the development of modern theoretical approaches. A good agreement between theoretical predictions and experimental data has been achieved for several defects in GaN, such as C_{N} , Zn_{Ga} , and Mg_{Ga} acceptors, responsible for the YL1, BL1, and UVL bands with the maxima at 2.2, 2.9, and 3.27 eV, respectively [2,4]. It should be noted that in some cases, such as Mg_{Ga} , theory predicts two different acceptor states, one of which (shallow state) agrees with the experiment, while the other (deep state) is absent from it. Searching for other acceptors with deep levels, we have found a disagreement between theory and experiment for the calcium in gallium site (Ca_{Ga}) defect. Early first-principles calculations using density-functional theory in the local density approximation predicted the $-/0$ transition level of the Ca_{Ga} acceptor at 0.62–0.64 eV. However, according to the most recent calculations using hybrid functionals [5,6], the $-/0$ transition level of the Ca_{Ga} acceptor is at 1.01 eV above the valence-band maximum (VBM). Electron transitions via this level are expected to cause a PL band with a maximum at 2.07 eV [6]. These predictions disagree with the published PL results, yet the experimental data are scarce.

Pankove and Hutchby [7] studied PL from GaN implanted with Ca and found a broad band with a maximum at 2.50 eV and full width at half maximum (FWHM) of 0.53 eV at $T = 78$ K. Monteiro *et al.* [8] implanted Ca in GaN grown by molecular-beam epitaxy (MBE) and annealed the sample in N_2 at 1050 °C for 15 min. A strong green PL band was observed with a maximum at 2.5 eV at $T = 14$ K (2.59 eV at room temperature), yet several weaker broad PL bands (at 2.95, 2.36, and 1.8 eV) were also detected after Ca implantation. The authors of Ref. [8] proposed that the green band at 2.59 eV is caused by transitions from a deep donor at 0.6 eV below the conduction band to the acceptor level at 0.3 eV above the VBM. Alves *et al.* [9] suggested that the broad band at 2.5 eV at $T = 14$ K consisted of two bands—at 2.36 and 2.59 eV. Chen and Skromme [10] observed only a green band at 2.35 eV after implantation of Ca, very similar to PL from implanted Mg and Zn. Godlewski *et al.* [11] studied PL from bulk GaN doped with Ca and observed only a yellow band with a maximum at about 2.2 eV at $T = 2$ K. The review of the above works shows no consensus in identifying PL bands related to Ca and sets a puzzle on where the Ca_{Ga} transition level is.

The practical importance of studying Ca in GaN is also related to the fact that Ca is potentially a source of nonradiative recombination that detrimentally affects the efficiency of III-nitride-based light-emitting devices [5,12]. Contamination of GaN or InGaN with Ca could pose a serious problem, especially in devices fabricated by using the MBE technique. Young *et al.* [12] investigated MBE-grown GaN and InGaN layers deposited on top of GaN/sapphire substrates grown by metal-organic chemical vapor deposition (MOCVD). From secondary ion mass spectrometry (SIMS) measurements, the concentration of Ca was below the detection limit (10^{13} cm⁻³) in the MOCVD GaN substrate; however, it increased to

TABLE I. Parameters of representative GaN samples implanted with Ca.

Sample		Implantation			Annealing					
Name	Group	Number	Substrate	E (keV)	Dose (cm^{-2})	T ($^{\circ}\text{C}$)	T_{ann} ($^{\circ}\text{C}$)	Time (min)	AlN cap	Pres-sure (atm)
A	I	Ca-R-2	GaN:Si	180	10^{14}	30	1100	10	No	1
B	I	s1481	GaN:Si	180	10^{14}	30	1100	60	Yes	1
C	I	s1486	GaN:Si	180	10^{14}	500	1100	240	Yes	1
D	I	Ca-R-1400	GaN:Si	180	10^{14}	30	1400	30	No	1 GPa
E	II	s1676f	u-GaN	190	10^{12}	600	1200	60	Yes	1
F	II	s1679d	GaN:Si	190	10^{12}	600	1100	60	Yes	1
G	II	s1679f	GaN:Si	190	10^{12}	600	1200	60	Yes	1

$8 \times 10^{15} \text{ cm}^{-3}$ in the n -type MBE GaN layer grown at $T = 820^{\circ}\text{C}$ and 10^{18} cm^{-3} in InGaN/GaN quantum wells grown at 600°C . The authors of Ref. [12] proposed that Ca impurities in the MBE-grown GaN and InGaN originate from surface contamination (possibly from deionized water) of the GaN substrates, despite the careful cleaning procedures. They did not find Ca in GaN grown by MOCVD and explained it by much higher growth temperatures. High concentrations of Ca were also found by other researchers in unintentionally doped GaN grown by MBE at $T = 700\text{--}730^{\circ}\text{C}$ [13,14]. These publications gave us an insight that Ca is responsible for the aquamarine luminescence (AL) band with a maximum at 2.55 eV in GaN grown at low temperatures ($\sim 600^{\circ}\text{C}$) by MBE [3,15,16].

This paper presents the detailed study of PL from GaN implanted with Ca. We also identified the Ca-related green PL band with a maximum at 2.5 eV in undoped GaN grown by MBE. The experimental results are compared with first-principles calculations using the Heyd-Scuseria-Ernzerhof (HSE) hybrid functional tuned to fulfill the generalized Koopmans condition, and a reasonable agreement is achieved.

II. METHODS

A. Samples

The Ca ion implantation was performed at CuttingEdge Ions, LLC. The original 2-in. GaN wafers were grown on c -plane sapphire by hydride vapor-phase epitaxy (HVPE) technique at Kyma Technologies. Some GaN layers were undoped (u-GaN, with the room-temperature concentration of free electrons, n , lower than 10^{17} cm^{-3}), and others were doped with Si (GaN:Si, with $n \approx 10^{18} \text{ cm}^{-3}$). In total, 26 samples implanted with different doses/energies of Ca and annealed in different conditions were studied in detail by PL. Parameters of representative samples to be analyzed in this paper are shown in Table I.

The samples from group I (A–D) were implanted with $^{40}\text{Ca}^+$ ions at room temperature and $T = 500^{\circ}\text{C}$ with Ca ion energy and dose fixed at 180 keV and 10^{14} cm^{-2} , respectively. The peak concentration of Ca in these samples is approximately 10^{19} cm^{-3} at a depth of 100 nm. The samples of group II (E–G) were first capped with a 70-nm-thick AlN layer and then implanted with Ca at $T = 600^{\circ}\text{C}$ with Ca ion energy of 190 keV and a dose of 10^{12} cm^{-2} . The peak concentration of

Ca in these samples is approximately 10^{17} cm^{-3} at a depth of 55 nm (after AlN removal). Several samples of group I were annealed uncapped under atmospheric N_2 pressure at temperatures (T_{ann}) of 950 and 1100°C for 10 min (representative sample A). Alternatively, an AlN cap was deposited, and the samples were annealed for 1 h (sample B) or 4 h (sample C) at $T_{\text{ann}} = 1100^{\circ}\text{C}$. Some samples of group I were annealed uncapped at temperatures from 1250 to 1400°C with the ultrahigh-pressure annealing (UHPA) method at the Institute of High Pressure Physics in Poland (representative sample D) [17]. The samples of group II (E–G) remained capped with AlN after the implantation and were annealed at $T_{\text{ann}} = 1100$ and 1200°C for 1 h or at 1300°C for 30 min.

The Ca-related green PL band was also found in unintentionally doped GaN samples grown in 2001 by MBE at $T = 620\text{--}720^{\circ}\text{C}$ on top of HVPE GaN substrates [Professor Morkoç's group, Virginia Commonwealth University (VCU)] [15,16]. Now, we conducted more detailed PL studies for two of these samples. In sample MBE-1 (the original name is svt848), a region close to the sample's edge showed bright-green PL. Another sample (MBE-2 or svt890) is included in the analysis because it has a very low concentration of defects, while the Ca-related green PL band can be reliably identified, and important parameters of the defect can be found with higher accuracy.

B. Measurement details

Steady-state PL (SSPL) and time-resolved PL (TRPL) were excited with HeCd and nitrogen lasers, respectively [2,18,19]. The PL was dispersed by the 1200-rules/mm diffraction grating in a 0.3-m monochromator and detected by a Peltier-cooled photomultiplier tube. The neutral density filters were used to attenuate the excitation intensity, P_{exc} , in the range from 10^{-6} to 0.13 W/cm^2 . A closed-cycle optical cryostat was used for the temperature range from 18 to 320 K. The as-measured PL spectra were corrected for the measurement system's spectral response, and PL intensity was additionally multiplied by λ^3 , where λ is the light wavelength, to present the PL spectra in units proportional to the number of emitted photons as a function of photon energy [19]. The PL from the samples was measured under identical conditions. The internal quantum efficiency (IQE) for each PL band, η_i , was found by comparing the intensity after integrating over PL band with that from calibrated GaN samples [2,20,21].

C. Photoluminescence analysis

Quantitative analysis of SSPL and TRPL data obtained in a wide range of excitation intensities and temperatures allows one to find important parameters of point defects responsible for PL bands [2,3]. These include the electron- and hole-capture coefficients (C_n and C_p , respectively) and thermodynamic charge transition level, often associated with the zero-phonon line (ZPL) of PL.

The C_n can be found from PL lifetime τ_0 when PL is caused by electron transitions from the conduction band to the defect level, as

$$C_n = \frac{1}{n\tau_0}, \quad (1)$$

where the concentration of free electrons (n) can be determined from the Hall effect measurements. After the C_n is determined for a particular PL band, it can be used as a standard to find n in other GaN samples where the PL band is recognized, and TRPL measurements are conducted.

The C_p can be found from the temperature dependences of the PL intensity, I^{PL} , and/or PL lifetime τ . The I^{PL} commonly decreases exponentially with increasing temperature T above a critical temperature T_0 , a process called the PL quenching. For most of the defects in n -type GaN, the PL quenching is caused by the thermal emission of holes from the defect level to the valence band (the Schön-Klasens mechanism) [22]. For PL caused by transitions from the conduction band to the defect level, the $I^{PL}(T)$ and $\tau(T)$ dependences can be described with the following expressions [18,21]:

$$I^{PL}(T) = \frac{I^{PL}(0)}{1 + C \exp\left(\frac{-E_A}{kT}\right)} \quad (2)$$

and

$$\tau(T) = \frac{\tau_0}{1 + C \exp\left(\frac{-E_A}{kT}\right)}, \quad (3)$$

with $C = (1-\eta_0)\tau_0 C_p N_v g^{-1}$. Here, $I^{PL}(0)$, η_0 and τ_0 are the PL intensity, IQE, and PL lifetime, respectively, at $T < T_0$; N_v is the effective density of states in the valence band (we assumed $N_v = N'_v T^{3/2}$ with $N'_v = 3.15 \times 10^{15} \text{ cm}^{-3} \text{ K}^{-3/2}$ for GaN); k is the Boltzmann constant; and g is the degeneracy of the defect level (assumed $g = 2$). The E_A in these expressions is the activation energy (the defect ionization energy), which is equal to the distance from the defect level to the valence band plus a potential barrier for the hole capture if any.

For semi-insulating (SI) GaN, the abrupt and tunable quenching mechanism is common [21]. The $I^{PL}(T)$ dependence can be formally described with Eq. (2), yet in this case the parameters C and E_A do not have any physical meaning. The E_A may greatly exceed the real activation energy (the abrupt quenching), and T_0 increases with P_{exc} (i.e., tunable quenching). For such samples, the defect ionization energy can be found from the following expression [21]:

$$E_A = kT_0 \ln\left(\frac{B'}{P_{exc}}\right), \quad (4)$$

where B' is a parameter depending on C_p and relative concentrations of defects participating in charge-carrier recombination. The abrupt and tunable quenching is reminiscent

of a phase transition: At $T < T_0$ the recombination efficiency is dictated by defects that capture holes more efficiently, whereas at $T > T_0$ the defects that capture electrons faster become the dominant recombination channels.

The parameters related to the electron-phonon coupling for the defect can be estimated from the PL band shape. The shape of a defect-related PL band can be fitted with the following expression obtained in a one-dimensional configuration coordinate model [23]:

$$I^{PL}(\hbar\omega) = I^{PL}(\hbar\omega_{\max}) \exp\left[-2S_e \left(\sqrt{\frac{E_0^* - \hbar\omega + \Delta}{d_{FC}^g}} - 1\right)^2\right]. \quad (5)$$

Here, S_e is the Huang-Rhys factor in the excited state of the defect, $d_{FC}^g = E_0^* - \hbar\omega_{\max}$ is the Frank-Condon shift in the ground state, $E_0^* = E_0 + 0.5\hbar\Omega_e$, E_0 is the ZPL energy, $\hbar\Omega_e$ is the energy of the effective phonon mode in the excited state, and $\hbar\omega$ and $\hbar\omega_{\max}$ are the photon energy and position of the PL band maximum, respectively. The Δ is a small shift of the PL band maximum due to sample-dependent reasons such as in-plane biaxial strain in thin GaN layers grown on sapphire substrates or local electric fields. The $\hbar\Omega_e$ can be determined from the temperature dependence of the PL band FWHM, W . In a simple model, it is described with the following expression [3,23]:

$$W(T) = W(0) \sqrt{\coth\left(\frac{\hbar\Omega_e}{2kT}\right)}. \quad (6)$$

Analysis of PL also reveals the type of electron transitions [2]. In n -type GaN, the majority of PL bands at low temperatures ($T < 50 \text{ K}$) are caused by electron transitions from shallow donors to various acceptors, the so-called donor-acceptor pair (DAP) recombination. The PL intensity after a laser pulse decays nonexponentially in this case. At higher temperatures, transitions from the conduction band to the same acceptors (the eA transitions) replace the DAP transitions. The PL decay becomes exponential, with the characteristic time τ_0 , which is inversely proportional to the concentration of free electrons; see Eq. (1). The PL from donors in GaN is usually caused by internal transitions: from an excited state of a positively charged donor to the ground state [2]. In this case, the PL decay is exponential even at very low temperatures, and it is independent of n .

Finally, the concentrations of defects N can be found from the dependence of PL intensity on the excitation photon flux, P , [24]:

$$\frac{I^{PL}(P)}{I_0^{PL}} = \frac{\eta(P)}{\eta_0} = \frac{P^{cr}}{P} \ln\left(1 + \frac{P}{P^{cr}}\right), \quad (7)$$

with $P^{cr} = N(\eta_0\alpha\tau_0)^{-1}$. Here, η_0 and I_0^{PL} are the IQE and PL intensity, respectively, in the limit of low excitation intensity, and α is the absorption coefficient for the incident photons ($1.2 \times 10^5 \text{ cm}^{-1}$ at 325 nm) [25].

D. Calculation details

Theoretical calculations were performed using the HSE hybrid functional [26]. The HSE functional parametrization used in this work fulfills the generalized Koopmans condition

TABLE II. Defect-related PL bands and parameters in Eq. (5) defining the bands' positions and shapes

PL band	Attribution	E_0^* (eV)	S_e	d_{FC}^g (eV)
GL _{Ca}	Ca _{Ga}	3.02	8.5	0.53
GL2	V _N	2.85	26.5	0.52
YL1	C _N	2.67	7.5	0.50

for the localized defect state of the Ca_{Ga} acceptor (fraction of exact exchange is 0.25; the range separation parameter is 0.161 Å⁻¹). The same parametrization also fulfills the generalized Koopmans condition and was used for calculations of Mg_{Ga} and Be_{Ga} acceptors [27,28], as well as several other defects and complexes in GaN [29]. This parametrization of HSE underestimates the bulk band gap of GaN, yielding 3.22 eV. Therefore, an experimental band gap of GaN (3.5 eV) was used to compare the defect optical transitions with measurements. Since transition levels are obtained with respect to the top of the valence band, this amounts to an upward shift of the conduction band. This is justified by the fact that acceptor levels closely follow the valence band as HSE parameters are varied [30]. Calculations were performed in 300-atom hexagonal supercells at the Γ point, with plane-wave energy cutoffs of 500 eV. All defect atomic structures were relaxed using HSE to minimize forces to 0.05 eV/Å or less. Artificial electrostatic interactions in calculated total energies were corrected using the Freysoldt-Neugebauer-Van de Walle approach [31,32]. Adiabatic potentials used to plot the configuration coordinate diagrams were obtained by fitting into HSE-computed total energies using harmonic approximation.

III. EXPERIMENTAL RESULTS

A. GaN implanted with Ca

In PL spectra from all 26 GaN samples implanted with Ca and annealed in different conditions, the green luminescence (GL_{Ca}) band with a maximum at about 2.5 eV was found. The intensity of this band and the presence of other PL bands depend on the implantation and annealing conditions (Table I).

1. Samples with a high concentration of Ca (group I)

Low-temperature PL spectra from representative samples of group I are shown in Fig. 1. In most samples implanted with a high dose of Ca, a red band (labeled RL_{Ca}) with a maximum at 1.8 eV and a green band (GL2) with a maximum at 2.35 eV are the strongest PL bands. At $T = 18$ K, the PL intensity of the RL_{Ca} and GL2 bands decays exponentially after a laser pulse, with the characteristic times of 2 and 0.25 ms, respectively. The GL2 band is caused by the isolated nitrogen vacancy (V_N) [23], whereas the RL_{Ca} band is attributed to the V_NCa_{Ga} complex [33]. The properties of the RL_{Ca} band and other red bands associated with the V_NA complexes (where A = Be_{Ga}, Mg_{Ga}, and Ca_{Ga}) will be discussed in detail elsewhere [33]. The GL2 band is observed only in semi-insulating GaN samples [2].

The GL_{Ca} band in samples of group I annealed at atmospheric N₂ pressure (samples A, B, and C) is commonly

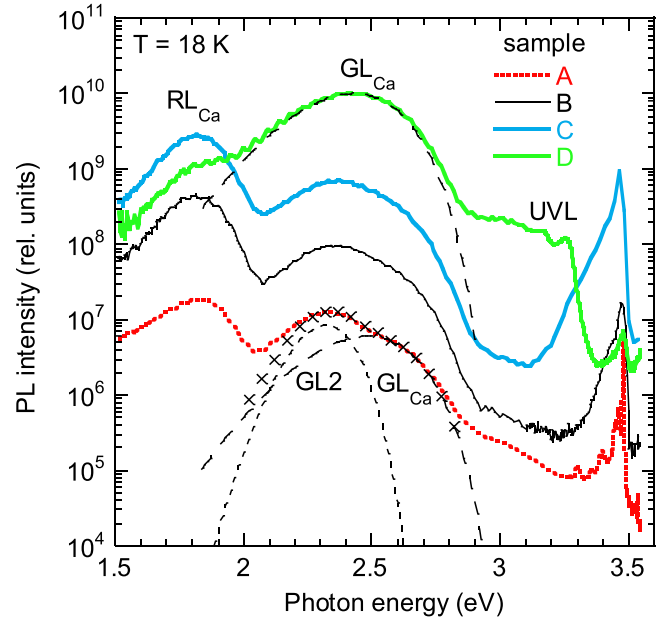


FIG. 1. PL spectra from GaN implanted with Ca (group I). $T = 18$ K and $P_{\text{exc}} = 10^{-4}$ W/cm². The PL spectra are measured in identical conditions and plotted in relative units. The dashed lines are calculated using Eq. (5) with S_e , E_0^* , and d_{FC}^g given in Table II. $\Delta = -0.06$ eV for sample D and $\Delta = -0.01$ eV for sample A. The \times symbols show the sum of the calculated curves for sample A.

observed as a shoulder at the high-energy side of the GL2 band. The deconvolution of the PL spectrum (an example is shown in Fig. 1) allows us to resolve the GL2 and GL_{Ca} bands and determine their contributions at different intensities and temperatures. With increasing temperature, the GL2 band is quenched above 100 K with the activation energy of ~ 0.1 eV, and the GL_{Ca} band is quenched above 200 K with the activation energy of 0.4–0.5 eV. Note that the accuracy of the E_A obtained from Eq. (2) is low for these samples because of the significant overlap of the PL bands.

The intensity of the GL_{Ca} band is much higher in samples annealed by the UHPA method (sample D in Fig. 1 with an IQE of about 0.5). No GL2 band could be found in sample D, although a small contribution of the GL2 band was observed in GaN annealed by UHPA at 1250 °C. The absence of the GL2 band and a relatively weak RL_{Ca} band in GaN annealed under ultrahigh N₂ pressure are explained by a significant reduction of the nitrogen vacancies concentration in these samples. The shape of the GL_{Ca} band is fitted with Eq. (5) in Fig. 1 with parameters given in Table II.

All the samples with a high concentration of implanted Ca show semi-insulating behavior. In such samples, the abrupt and tunable quenching of PL is common [2,21,22,34]. Since the GL_{Ca} band is strong and well resolved in sample D, its quenching behavior can be studied in detail. The temperature dependencies of the peak PL intensity at selected excitation intensities are shown in Fig. 2.

The PL intensity decreases above critical temperature T_0 . The quenching is abrupt (the apparent “activation energy” is about 800 meV) and tunable by the excitation intensity (Fig. 2). The abrupt and tunable quenching in semi-insulating

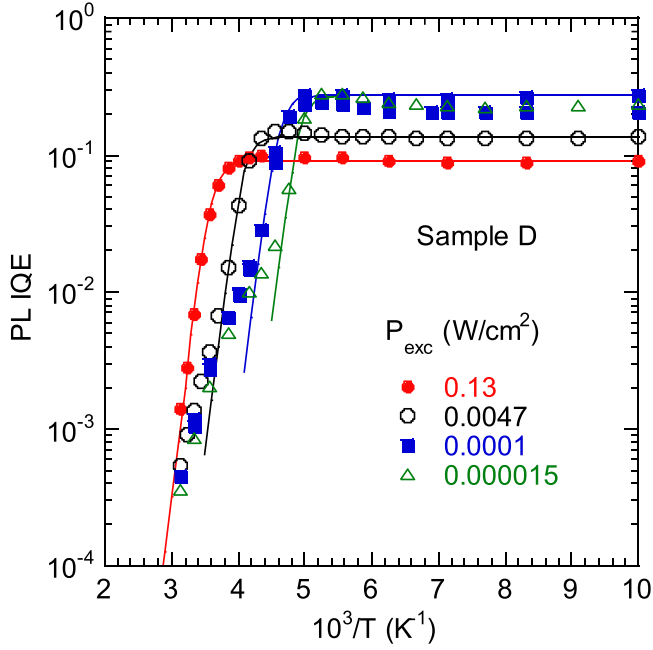


FIG. 2. Temperature dependence of the quantum efficiency of the GL_{Ca} band in sample D for selected excitation intensities. The solid lines are calculated using Eq. (2) with $C = 3.5 \times 10^{14}$, 2.7×10^{16} , 3.5×10^{18} , and 6×10^{19} for $P_{exc} = 0.13$, 4.7×10^{-3} , 1×10^{-4} , and 1.5×10^{-5} W/cm², respectively, and $E_A = 800$ meV for all the curves.

semiconductors is explained by a sudden switch from the population inversion to a quasiequilibrium population of energy levels in the band gap [21]. The drop of PL intensity at T_0 is abrupt, resembling a phase transition. In such samples, the ionization energy of the acceptor can be found from Eq. (4) [2,21]. For sample D, $E_A = 0.55 \pm 0.05$ eV. Note that the ionization energy determined by this method is sometimes overestimated [35,36].

2. Samples with a low concentration of Ca (group II)

The samples implanted with a low dose of Ca (group II in Table I) behave as conductive n type. From the analysis of TRPL at different temperatures, we determined that $n = 1 \times 10^{18}$ cm⁻³ and 1.3×10^{18} cm⁻³ in samples F and G, respectively, at $T = 100$ K, and $n = 1.6 \times 10^{16}$ cm⁻³ in sample E at $T = 300$ K (Table III). Figure 3 shows PL spectra at 18

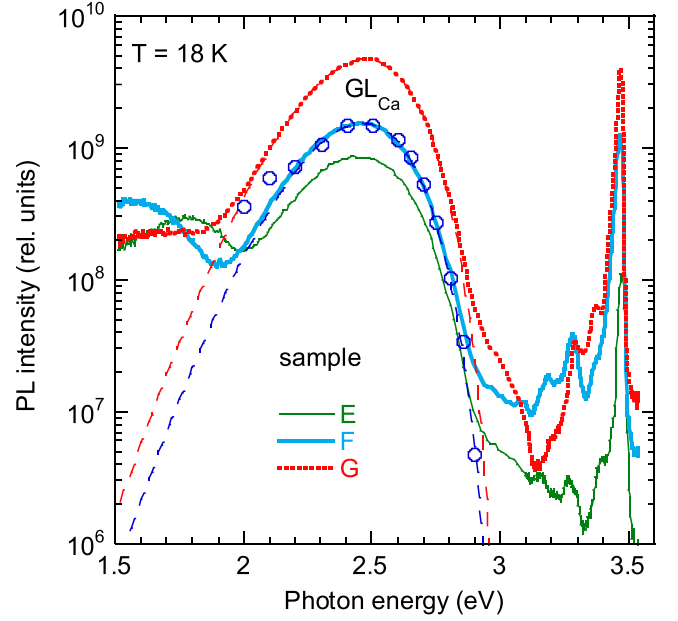


FIG. 3. PL spectra from GaN implanted with Ca (group II). $T = 18$ K and $P_{exc} = 10^{-4}$ W/cm². The PL intensity is in the same relative units as in Fig. 1. The dashed lines are calculated using Eq. (5) with S_e , E_0^* , and d_{FC}^2 given in Table II. $\Delta = -0.016$ eV for sample G and $\Delta = -0.026$ eV for sample F. The circles show the TRPL spectrum for sample F at a time delay of 20 μ s shifted vertically to match the SSPL spectrum.

K from representative GaN samples. In samples annealed at 1100 and 1200 °C, the donor-bound exciton (DBE) band has a maximum at 3.478 eV and FWHM = 4.5 meV (Ca implanted in undoped GaN) and 3.475 eV and FWHM = 11 meV (Ca in Si-doped GaN). A small blueshift of the exciton lines (by 4–7 meV) is caused by biaxial strain in GaN grown on sapphire substrates.

All the samples reveal the GL_{Ca} band with a maximum at about 2.5 eV, attributed to the Ca_{Ga} acceptor. The shape of the GL_{Ca} band was fitted with Eq. (5), and the following parameters were found: $S_e = 8.5$, $E_0^* = 3.02$ eV, and $\hbar\omega_{max} = 2.49$ eV. Note that acceptable agreement with the experimental data can be achieved if the S_e and E_0^* are varied simultaneously (from 6.9 and 2.97 eV to 10.4 and 3.07 eV), which results in the following uncertainty ranges: $S_e = 8.5 \pm 1.7$ and $E_0^* = 3.02 \pm 0.05$ eV.

TABLE III. The parameters of selected samples and parameters of the GL_{Ca} band in GaN.

Sample	[Ca] (cm ⁻³)	n (cm ⁻³) at $T = 100$ K	η (GL_{Ca}) at $T = 100$ K	τ (s) at $T = 100$ K	C_n (cm ³ /s)	C_p (cm ³ /s)	E_A (eV)
D	$\sim 7 \times 10^{18}$	SI	0.5	Nonexp.	$(7 \pm 3) \times 10^{-14}$		0.55 ± 0.05^a
E	$\sim 7 \times 10^{16}$	7×10^{15}	0.05	1.5×10^{-3}		$(1.1^{+2.9}_{-0.8}) \times 10^{-6}$	0.47 ± 0.03^b
F	$\sim 7 \times 10^{16}$	1×10^{18}	0.1	1.5×10^{-5}			
G	$\sim 7 \times 10^{16}$	1.3×10^{18}	0.3	1.2×10^{-5}			0.50 ± 0.02^c
MBE-1	2×10^{16}	3×10^{17}	0.2	3.5×10^{-5}			
MBE-2	5×10^{14}	9×10^{15}	0.04	1.2×10^{-3}	$(9.5 \pm 2) \times 10^{-14}$	$(6 \pm 2) \times 10^{-7}$	0.49 ± 0.01^b

^aFrom the fit of the $T_0(P_{exc})$ dependence with Eq. (4).

^bFrom the fit of the $I^{PL}(T)$ dependence with Eq. (2).

^cFrom the fit of the $I^{PL}(\hbar\omega)$ dependence with Eq. (5)

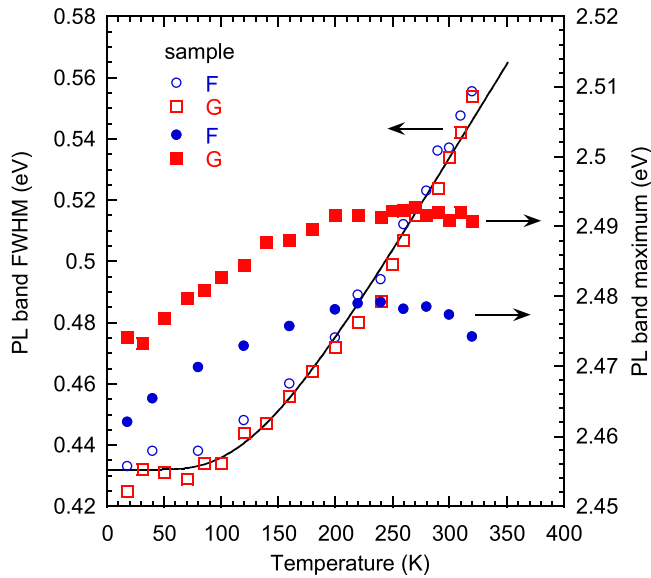


FIG. 4. The temperature dependences of the FWHM and $\hbar\omega_{\max}$ for the GL_{Ca} band in GaN:Si implanted with Ca and annealed at 1100 and 1200 °C. $P_{\text{exc}} = 6.5 \times 10^{-4} \text{ W/cm}^2$. The FWHM is fitted using Eq. (6) with the following parameters: $W(0) = 0.432 \text{ eV}$, $\hbar\Omega_e = 40.5 \text{ meV}$.

In samples of group II, the GL_{Ca} band is well resolved (compare Fig. 3 with Fig. 1), so that the temperature dependence of its shape and position can be reliably determined. With increasing temperature, the GL_{Ca} band shifts to higher photon energies and broadens (Fig. 4). The behavior was reproducible in several GaN:Ca samples. The FWHM of the PL band, W , increases from 0.43 eV at $T = 18 \text{ K}$ to 0.56 eV at $T = 320 \text{ K}$. The dependence is fitted with Eq. (6) with the effective phonon energy $\hbar\Omega_e$ as the only fitting parameter (Fig. 4). The obtained value of $\hbar\Omega_e = 40 \text{ meV}$ is typical for acceptors in GaN [3].

The temperature dependence of the PL intensity (in arbitrary units) and PL lifetime for the GL_{Ca} band in samples E and G are shown in Fig. 5. PL lifetime for the GL_{Ca} band did not change with increasing T from 40 to 100 K in samples F and G (16 and 12 μs , respectively), indicating that these samples are degenerate n type. The decay of the GL_{Ca} intensity in sample E is nonexponential at temperatures below 240 K. This observation agrees with a very low concentration of free electrons in this sample ($n = 1.6 \times 10^{16} \text{ cm}^{-3}$ at $T = 300 \text{ K}$) and the expected predominance of the DAP-type recombination. The effective lifetime was estimated with the method suggested in Ref. [37]. The dependences are fitted with Eqs. (2) and (3), and an example is shown in Fig. 5. The $\tau(T)$ dependence for sample E has a wide range and thus provides the most reliable values of the fitting parameters. We obtained $E_A = 0.47 \pm 0.03 \text{ eV}$ and $C_p = (1.1^{+2.9}_{-0.8}) \times 10^{-6} \text{ cm}^3/\text{s}$. For other samples, the uncertainty of the parameters is much larger.

3. Effect of excitation intensity on the GL_{Ca} band

The above analysis of PL spectra was conducted at low excitation intensities to avoid the saturation of defect-related

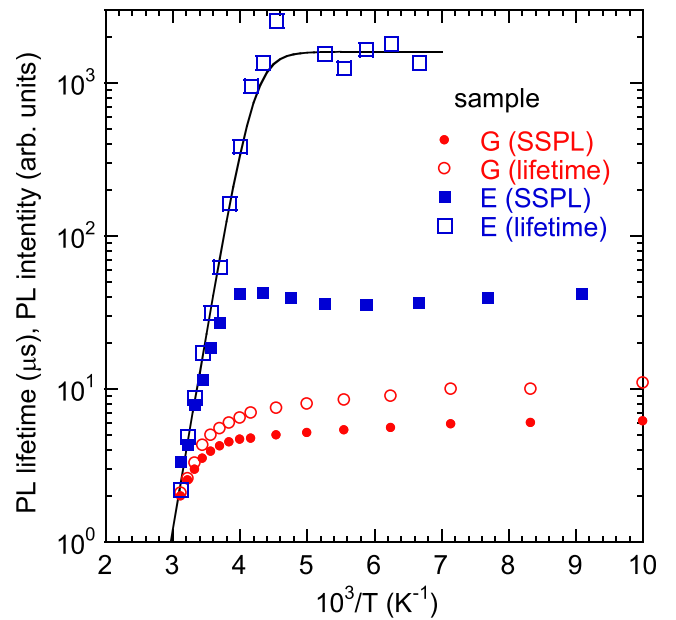


FIG. 5. Temperature dependence of PL intensity and PL lifetime for sample E (undoped GaN implanted with Ca and annealed at 1200 °C) and sample G (Si-doped GaN implanted with Ca and annealed at 1200 °C). The PL intensities are shifted vertically to match the $\tau(T)$ dependences in the region of PL quenching. The line is calculated using Eq. (3) with the following parameters: $\eta_0 = 0.1$, $C_p = 1.1 \times 10^{-6} \text{ cm}^3/\text{s}$, $\tau_0 = 1.6 \text{ ms}$, and $E_A = 0.47 \text{ eV}$.

PL. We noticed that at low excitation intensities, the GL_{Ca} band position slightly differs from sample to sample (different Δ), whereas its shape is invariant (Figs. 1, 3, and 4). The dependence of the GL_{Ca} band maximum on excitation intensity for selected samples is shown in Fig. 6.

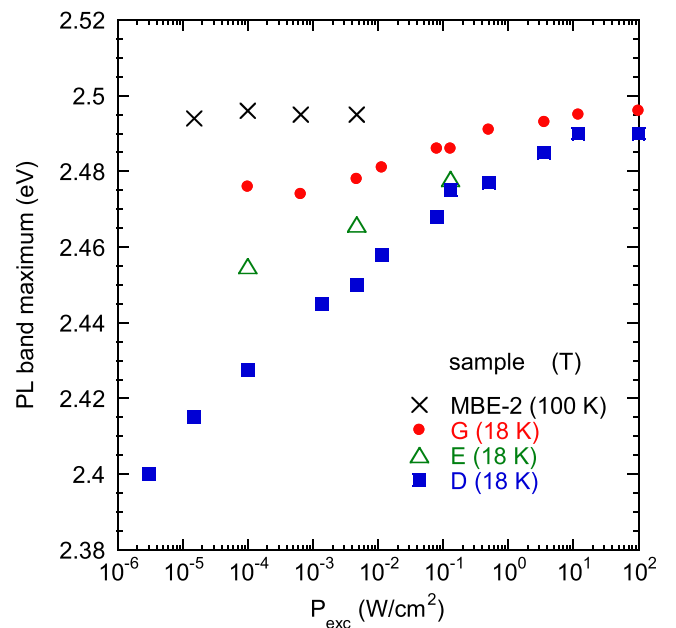


FIG. 6. The dependence of the GL_{Ca} band maximum on excitation intensity.

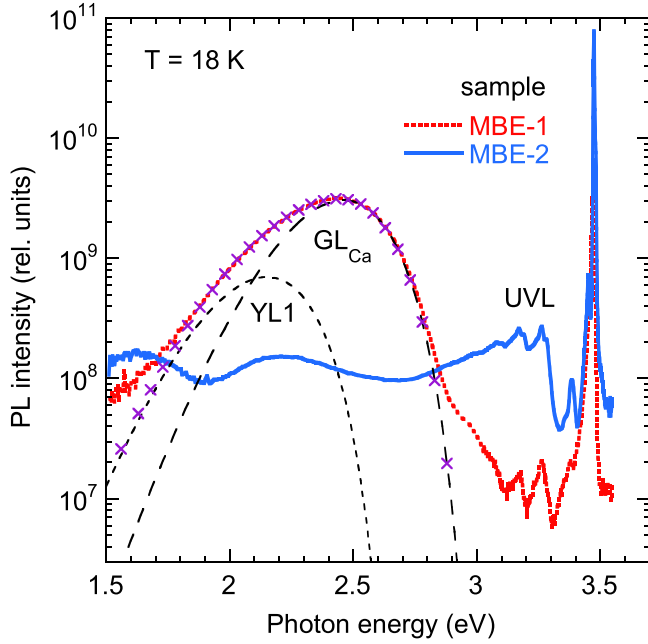


FIG. 7. PL spectrum from MBE GaN samples at $T = 18$ K and $P_{\text{exc}} = 1 \times 10^{-4}$ W/cm 2 . The dashed lines are calculated using Eq. (5) with S_e , E_0^* , and d_{FC}^s given in Table II. $\Delta = -0.03$ eV for the GL_{Ca} band, and $\Delta = -0.02$ eV for the YL1 band. The \times symbols show the sum of the two calculated curves.

For the n -type GaN sample (G), the total shift is about 20 meV with increasing P_{exc} from 10^{-4} to 100 W/cm 2 . This small shift can be explained by the DAP-type transition involving shallow donors and the Ca_{Ga} acceptor. The shift is larger for samples with a low concentration of n and semi-insulating samples (up to 0.1 eV). The large shifts are attributed to potential fluctuations or other sources of local electric fields in semi-insulating semiconductors [38]. After analyzing the $\hbar\omega_{\text{max}}(P_{\text{exc}})$ dependences in several samples, we concluded that $\hbar\omega_{\text{max}} = 2.49 \pm 0.01$ eV for transitions from the conduction band to the Ca_{Ga} acceptor in relaxed GaN free from electric fields.

B. Ca-related green band in undoped MBE GaN

Young *et al.* [12] have demonstrated that undoped GaN samples are contaminated with Ca (with concentrations up to 10^{18} cm $^{-3}$) when GaN is grown by the MBE method at low temperatures (600–800 °C). We assume that the AL band with a maximum at 2.56 eV observed in undoped MBE-grown GaN [3,15,16] is caused by the Ca_{Ga} acceptor and will provide the evidence for this assumption below.

At $T = 18$ K, the PL spectrum from the edge region of nominally undoped GaN (sample MBE-1) shows a strong green band (Fig. 7). The deconvolution of the PL spectrum at 18 K (shown with dashed lines) and other temperatures revealed the Ca_{Ga} -related GL_{Ca} band with a maximum at 2.46 eV and the C_N -related YL1 band with a maximum at 2.15 eV. The GL_{Ca} band is quenched at $T > 260$ K. Its shape and evolution with temperature are nearly identical to those in GaN implanted with Ca (Sec. III A). The parameters C_n and C_p estimated from Eqs. (1)–(3) are close to those found

for the Ca-implanted GaN samples, yet the accuracy of these parameters is still not high enough. Much higher accuracy can be achieved from the analysis of PL from sample MBE-2.

The low-temperature PL spectrum from sample MBE-2 contained a very strong exciton band and weak defect-related bands (Fig. 7). The strongest peak at 3.475 eV with the FMHM of 3.5 meV is identified as DBE, and a peak at 3.482 eV is attributed to the free exciton (FE). The assignments are confirmed by the evolution of the PL spectrum with temperature. The shift of the peaks by 4 meV from their positions in bulk GaN (3.471 and 3.478 eV) [3] is caused by a small biaxial strain. The two-electron satellite and longitudinal-optical (LO) phonon replicas of the DBE and FE peaks are observed and, along with high IQE and small FWHM, indicate a high quality of the GaN layer. The IQE of the exciton emission is estimated as 0.06 from a comparison of the integrated PL intensity with that of calibrated GaN samples (note that the relative efficiency of the near band-edge emission is typically underestimated because of the self-absorption effect [2]). The defect-related PL is very weak, with a total IQE of 0.04 in the limit of low excitation intensity at $T = 18$ K.

With increasing temperature from 18 to 100 K, the exciton emission intensity dramatically decreases, while the intensities of defect-related PL bands increase by a factor of ~ 5 . This transformation can result from competition for holes in n -type GaN, where the quenching of a recombination channel with IQE close to unity (the exciton emission in this case) results in the enhancement of emissions from other recombination channels [2]. At $T > 80$ K, the GL_{Ca} and YL1 bands can be reliably resolved in the PL spectrum (Fig. 8). The GL_{Ca} band is quenched at $T > 250$ K, while the YL1 band intensity does not change up to 320 K.

The temperature dependences of PL intensities and PL lifetimes for the GL_{Ca} and UVL bands in sample MBE-2 are shown in Fig. 9 and fitted with Eqs. (2) and (3). The quenching of the UVL and GL_{Ca} bands at $T_0 = 110$ and 240 K, respectively, and the quenching is not tunable. At $T < T_0$, the $I^{PL}(T)$ dependences are constant, in agreement with Eq. (2). The PL lifetime of both the UVL and GL_{Ca} bands slowly decreases with increasing temperature from 60 K to T_0 . This decrease is attributed to the temperature-induced increase in n , while the C_n in Eq. (1) is independent of temperature [24]. To fit the $\tau(T)$ dependences at $T < T_0$, the $n(T)$ dependence was simulated with the following equation [24,39]:

$$n = \frac{1}{2} \left[\sqrt{(\phi + N_A)^2 + 4\phi(N_D - N_A)} - (\phi + N_A) \right]. \quad (8)$$

Here, N_D and N_A are the concentrations of shallow donors and all acceptors, respectively, $\phi = N_C' T^{3/2} g^{-1} \exp(-E_D/kT)$, where $g = 2$, N_C' is the effective density of states in the conduction band at $T = 1$ K ($N_C' \approx 5 \times 10^{14}$ cm $^{-3}$ K $^{-3/2}$ for $m^* = 0.22m_0$), and E_D is the donor activation energy. From the best fit of the $\tau(T)$ dependence for the UVL band at $T < T_0$ using Eq. (1) with $C_n = 3.2 \times 10^{-12}$ cm 3 /s (shown with the dotted line in Fig. 9), we found the $n(T)$ dependence for this sample. In particular, $n = 9 \times 10^{15}$ cm $^{-3}$ at 100 K and $n = 1.5 \times 10^{16}$ cm $^{-3}$ at 300 K.

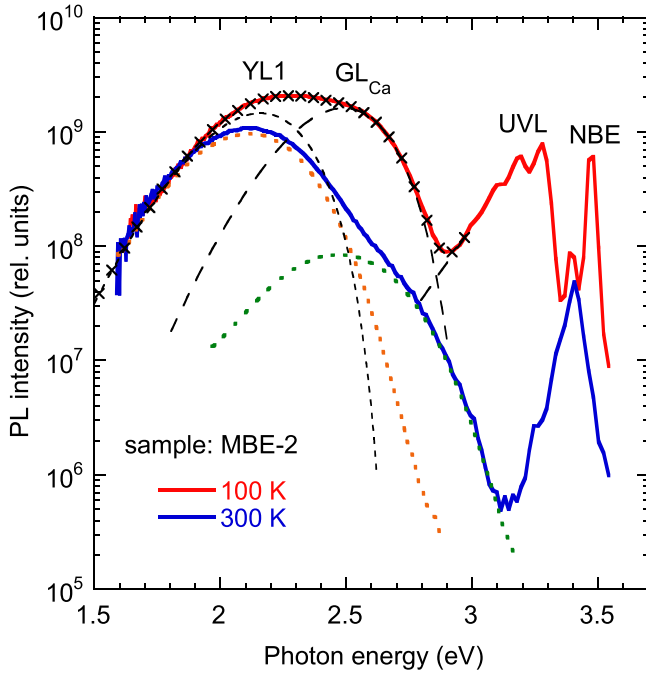


FIG. 8. PL spectrum from sample MBE-2 at $T = 100$ and 300 K and $P_{\text{exc}} = 2 \times 10^{-5} \text{ W/cm}^2$. The dashed lines show the shapes of the YL1 and GL_{Ca} bands at 100 K calculated using Eq. (5) with S_e , E_0^* , and d_{FC}^g given in Table II ($\Delta = 0$). The \times symbols show the sum of the calculated PL bands. The dotted line shows the typical shape of the YL1 band at 300 K in C-doped GaN samples.

By using the obtained $n(T)$ dependence, we fitted the $\tau(T)$ dependence for the GL_{Ca} band at $T < T_0$ and found $C_n = 9.5 \times 10^{-14} \text{ cm}^3/\text{s}$ for the Ca_{Ga} acceptor. The $\tau_0(T)$ dependences are shown with the dotted lines in Fig. 9. At $T > T_0$, the PL quenching and the decrease in PL lifetime practically coincide because the PL lifetime is nearly constant in the quenching region. From the fit of the $I^{\text{PL}}(T)$ and $\tau(T)$ dependences in the whole range of measured temperatures (solid lines in Fig. 9), we found $E_A = 190 \text{ meV}$ and $C_p = 1 \times 10^{-6} \text{ cm}^3/\text{s}$ for the UVL band and $E_A = 490 \text{ meV}$ and $C_p = 6 \times 10^{-7} \text{ cm}^3/\text{s}$ for the GL_{Ca} band.

The accuracy of the parameters E_A and C_p obtained from the temperature dependences of PL intensity and PL lifetime is limited by the fact that a small increase (decrease) in the E_A can be compensated by an increase (decrease) in the C_p , so that the agreement between the calculated and experimental data is acceptable. For example, a reasonable agreement is achieved for sample MBE-2 with the parameters $E_A = 0.52 \text{ eV}$, $C_p = 2 \times 10^{-6} \text{ cm}^3/\text{s}$ and $E_A = 0.46 \text{ eV}$, $C_p = 1.7 \times 10^{-7} \text{ cm}^3/\text{s}$. This demonstrates that this method is inaccurate and can lead to errors in C_p by up to an order of magnitude. The problem with uncertainty in the parameters E_A and C_p exists not only for PL results but also in deep-level transient-spectroscopy analysis [40]. The accuracy of these parameters, as will be shown below, can be improved with an analysis of the excitation intensity dependences.

At $T = 100 \text{ K}$, the decays of the UVL, GL_{Ca} , and YL1 bands in sample MBE-2 are nearly exponential, which indicates that these PL bands are caused by electron transitions

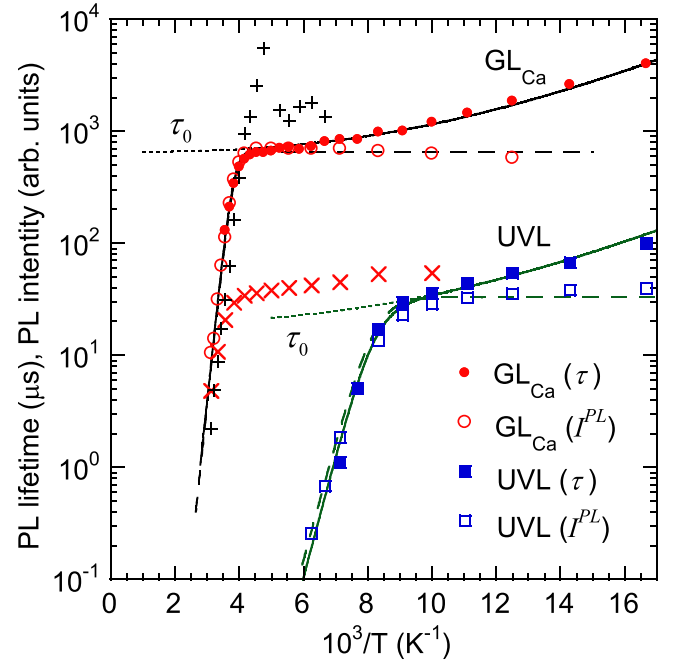


FIG. 9. Temperature dependence of PL intensity (at $P_{\text{exc}} = 2 \times 10^{-5} \text{ W/cm}^2$) and PL lifetime for the GL_{Ca} and UVL bands in sample MBE-2. The PL intensities are shifted arbitrarily to match the high-temperature portions of the $\tau(T)$ dependences. The solid lines are calculated using Eqs. (1) and (3) with the following parameters: $\eta_0 = 0.043$, $C_n = 0.95 \times 10^{-13} \text{ cm}^3/\text{s}$, $C_p = 6 \times 10^{-7} \text{ cm}^3/\text{s}$, and $E_A = 0.49 \text{ eV}$ for the GL_{Ca} band; $\eta_0 = 0.008$, $C_n = 3.2 \times 10^{-12} \text{ cm}^3/\text{s}$, $C_p = 1 \times 10^{-6} \text{ cm}^3/\text{s}$, and $E_A = 0.19 \text{ eV}$ for the UVL band. The dotted lines (coinciding with the solid lines at $T < T_0$) show the $\tau_0(T)$ dependences calculated using Eqs. (1) and (8) with the following parameters: $E_D = 20 \text{ meV}$, $g = 2$, $N_C' = 5 \times 10^{14} \text{ cm}^{-3} \text{ K}^{-3/2}$, $N_D = 2.6 \times 10^{16} \text{ cm}^{-3}$, $N_A = 1 \times 10^{16} \text{ cm}^{-3}$. The dashed lines for the $I^{\text{PL}}(T)$ dependences are calculated using Eq. (2) with the above parameters and $\tau_0 = 0.8 \text{ ms}$ for the GL_{Ca} band and $\tau_0 = 36 \mu\text{s}$ for the UVL band. The $+$ and \times symbols show the $\tau(T)$ dependence for samples E and MBE-1, respectively.

from the conduction band to the acceptor levels [2,3]. The PL lifetimes for these PL bands are 36 , 1150 , and $\sim 1000 \mu\text{s}$, respectively, at $T = 100 \text{ K}$. The $\eta(P)$ dependences are shown in Fig. 10.

By fitting these dependences with Eq. (7), we find that the concentration of the Ca_{Ga} defects is $4.5 \times 10^{14} \text{ cm}^{-3}$ in sample MBE-2. The concentrations of the C_{N} and Mg_{Ga} defects are also very low (6×10^{14} and $1 \times 10^{14} \text{ cm}^{-3}$, respectively), below the detection limit of SIMS. For sample MBE-1, the Ca_{Ga} concentration is determined as $2 \times 10^{16} \text{ cm}^{-3}$ with the same procedure, close to what was obtained in Ref. [16] for similar samples. The accuracy of these concentrations is limited by the accuracy of finding the absolute IQE, which is conservatively estimated as plus-minus half order of magnitude [41]. However, the relative concentrations of different types of defects in the same sample are found with much better accuracy because they depend on relative IQE (or integrated PL intensities).

After finding the relative concentrations of the defects responsible for the PL bands in sample MBE-2, we can

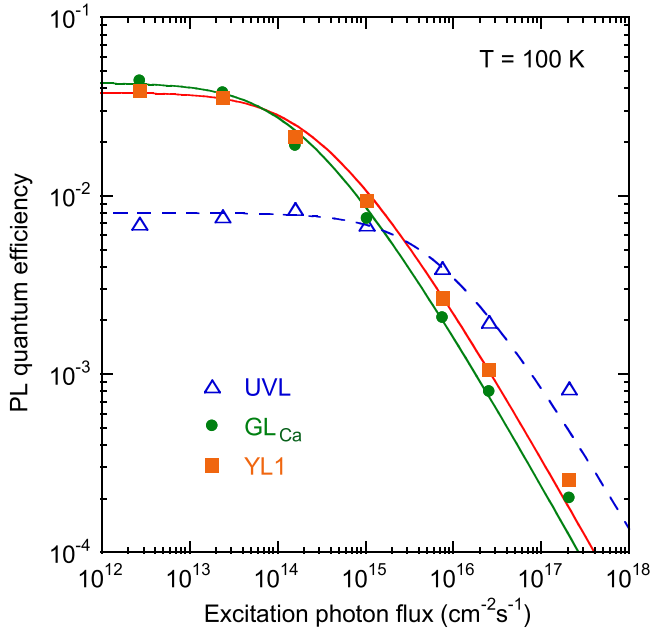


FIG. 10. Dependence of PL quantum efficiency on excitation intensity for PL bands in sample MBE-2 at $T = 100$ K. The lines are calculated using Eq. (7) with the following parameters: $N = 1 \times 10^{14} \text{ cm}^{-3}$, $\eta_0 = 0.008$, $\tau = 36 \mu\text{s}$ for the UVL band; $N = 4.5 \times 10^{14} \text{ cm}^{-3}$, $\eta_0 = 0.043$, $\tau = 1.2 \text{ ms}$ for the GL_{Ca} band; and $N = 6 \times 10^{14} \text{ cm}^{-3}$, $\eta_0 = 0.038$, $\tau = 1.0 \text{ ms}$ for the YL1 band. $\alpha = 1.2 \times 10^5 \text{ cm}^{-1}$.

fine-tune the hole capture coefficient for the Ca_{Ga} defect. Indeed, $C_{pi} = C_{pj}(N_j I_i^{PL}) / (N_i I_j^{PL})$ [2], where i is the defect with unknown C_p (Ca_{Ga}) and j is the defect with known C_p (C_{N} and Mg_{Ga}). By taking $C_p = (3.5 \pm 1.5) \times 10^{-7} \text{ cm}^3/\text{s}$ for the YL1 band and $C_p = (1.0 \pm 0.4) \times 10^{-6} \text{ cm}^3/\text{s}$ for the UVL band [2,34,41], and the I_i^{PL}/I_j^{PL} (or η_{0i}/η_{0j}) ratios from the experiment at $T = 100$ K, we find for the GL_{Ca} band that $C_p = (1.1 \pm 0.4) \times 10^{-6} \text{ cm}^3/\text{s}$ from comparison with the UVL band and $C_p = (0.5 \pm 0.2) \times 10^{-6} \text{ cm}^3/\text{s}$ from comparison with the YL1 band. We conclude that $C_p = (6 \pm 2) \times 10^{-7} \text{ cm}^3/\text{s}$ for the GL_{Ca} band. By using this C_p for the GL_{Ca} band in the fit of the $I^{PL}(T)$ dependence in Fig. 9, we obtain $E_A = 0.49 \pm 0.01 \text{ eV}$ for the GL_{Ca} band.

IV. THEORY

HSE calculations show that Ca_{Ga} is a deep acceptor, which forms the defect state localized on the nearest-neighbor nitrogen. Spin densities of two nonequivalent configurations of this defect state are shown in Fig. 11, i.e., showing two possible hole localizations on a neutral Ca_{Ga} acceptor. The energy of the hole localized along the wurtzite c axis [Fig. 11(a)] is 0.08 eV higher than that of the hole localized along one of the three equivalent in-plane nearest nitrogen atoms [Fig. 11(b)]. The optical transition energies via these defect states are also within less than 0.1 eV from each other. The configuration coordinate diagram in Fig. 12 is calculated for the lower-energy in-plane defect state [Fig. 11(b)]. In contrast to other group II acceptors in GaN, such as Mg_{Ga} and Be_{Ga} [27,28,42], we do not find a stable configuration of a weakly localized

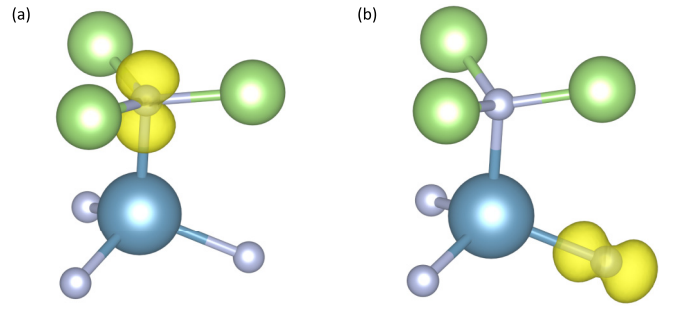


FIG. 11. Spin densities of the two configurations of the hole localized on the Ca_{Ga} acceptor in GaN. Isosurfaces of spin density at 10% of the maximum value are shown in yellow. The hole is localized along the wurtzite c axis (a); and along one of the three equivalent in-plane Ca-N bonds (b). The crystal structure of the Ca defect in GaN is shown as a ball and stick model, with the large blue spheres representing Ca atoms, medium green spheres are Ga , and small gray spheres are N atoms.

or anisotropically delocalized state for the Ca_{Ga} acceptor. Relaxation from various symmetry-breaking starting lattice structures leads to one of the two localized hole states shown in Fig. 11. The Ca-N in-plane bond lengths in Fig. 11(a) are 2.21 Å, while the c -axis Ca-N bond along which the hole is localized is extended to 2.31 Å. Similarly, in Fig. 11(b), the in-plane Ca-N bond where the hole is localized is 2.28 Å, the c -axis Ca-N bond is 2.24 Å, and the remaining in-plane Ca-N bonds are 2.21 Å.

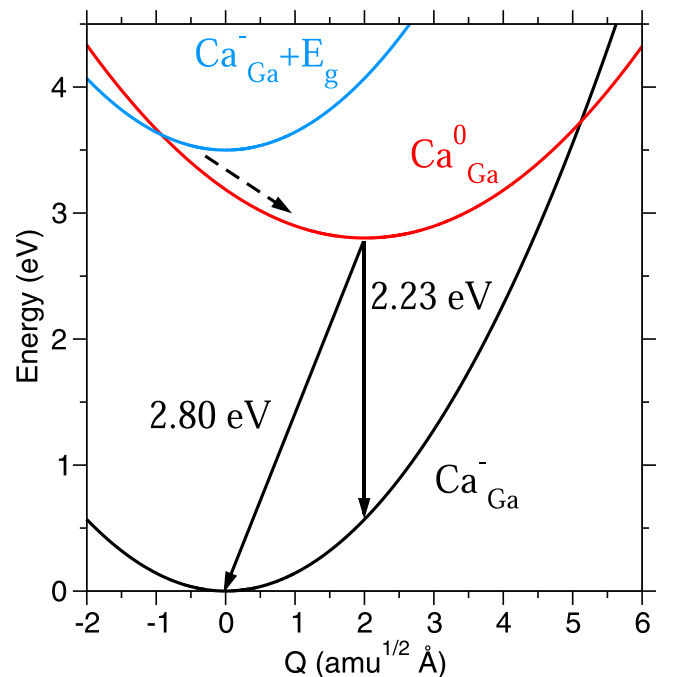


FIG. 12. Configuration coordinate diagram for the Ca_{Ga} defect in GaN. The adiabatic potentials are obtained by fitting into HSE-computed transition energies using harmonic approximation.

Optical transitions via Ca_{Ga} acceptor are illustrated using the configuration coordinate diagram in Fig. 12. The 0/− thermodynamic transition level for Ca_{Ga} acceptor is computed at 0.7 eV. Therefore, the acceptor is negatively charged for the Fermi levels above 0.7 eV, as shown by the lower adiabatic potential in Fig. 12. Direct vertical absorption energy for the Ca_{Ga} acceptor is calculated to be 3.2 eV, which could be revealed by below band-gap absorption experiments. In PL experiments performed in this work, the above band-gap excitation creates an electron-hole pair, which raises the energy of the system by the energy of the band gap (3.50 eV). The intersection of the neutral defect adiabatic potential with the upper potential of the negatively charged defect reveals a very low barrier (~ 0.1 eV) for the nonradiative hole capture, i.e., the transition from the negative to the neutral charge state of Ca_{Ga} . Nonradiative capture of the hole by the negative defect is shown with a dashed arrow in Fig. 12. From the neutral charge state, the path for the nonradiative recombination is blocked by a large potential barrier of about 0.9 eV, i.e., the barrier between the bottom of the neutral potential and the intersection of the neutral and lower negative potentials. Therefore, the recombination via the Ca_{Ga} acceptor is predominantly radiative. Direct vertical transition corresponding to the PL maximum is calculated to be 2.23 eV, while the ZPL for this PL band is predicted at 2.8 eV (Franck-Condon shift of 0.57 eV). (Note that for the c -axis localized acceptor state, the calculated PL maximum is at 2.3 eV, and the ZPL is at 2.9 eV). The HSE-calculated vibrational energies of the excited state (neutral Ca_{Ga}) and the ground state (negatively charged Ca_{Ga}) are $\hbar\Omega_e = 28.2$ meV and $\hbar\Omega_g = 34.4$ meV. The Huang-Rhys factor for the ground state can be obtained by dividing the Franck-Condon shift ($d_{FC}^g = 0.57$ eV) by the vibrational energy ($\hbar\Omega_g = 34.4$ meV): $S_g = 16.6$. Similarly, the Huang-Rhys factor for the excited state is obtained from the lattice relaxation energy following the resonant excitation (0.38 eV) and the vibrational energy of the excited state ($\hbar\Omega_e = 28.2$ meV): $S_e = 13.5$.

The calculated PL maximum and ZPL are by about 0.25 eV lower than those found experimentally. We suggest two possible reasons for this. First, there might be another (weakly) localized configuration of the hole on this acceptor, which is missing from our HSE calculations and is responsible for the observed PL band. This would be similar to the situation of Be_{Ga} and Mg_{Ga} acceptors in GaN, where the weakly localized states produce strong UVL bands, and HSE-predicted localized polaronic ground states are apparently not observed in PL spectra. Another possibility is that the HSE-obtained energies of polaronic defects states, despite being essentially self-interaction free in HSE tuning used here, contain an error, which leads to systematically shifted results compared to the experiment. Further research into these issues is needed to identify the sources of the disagreement.

V. DISCUSSION

The Ca-related green band (GL_{Ca}) with the maximum at 2.5 eV is found in GaN implanted with Ca and annealed in different conditions. The GL_{Ca} band is also present in undoped GaN grown at relatively low temperature by MBE and apparently contaminated with Ca, in agreement with earlier

findings [12–14]. An unidentified PL band with a maximum at 2.56 eV previously observed in GaN layers grown by MBE on freestanding HVPE-grown GaN substrates and named the AL band [15,16] is in fact the Ca-related GL_{Ca} band. A small difference in positions of the PL band maximum (2.50 vs. 2.56 eV) can be explained by less accurate calibration of the PL setup and not accounting for the λ^3 factor in previous works [2]. Analysis of n -type GaN samples with relatively low concentrations of Ca (implanted samples E, F, G, and undoped GaN sample MBE-2) provided the most valuable information about the defect responsible for the GL_{Ca} band.

The GL_{Ca} band is attributed to electron transitions from shallow donors (at $T < 50$ K) or from the conduction band (at $T > 50$ K) to the Ca_{Ga} acceptor. From the analysis of PL spectra and PL quenching, the −/0 transition level of the Ca_{Ga} acceptor is found at 0.50 ± 0.02 eV above the VBM at $T = 18$ K. In semi-insulating GaN samples implanted with high doses of Ca, the band maximum is redshifted by up to 0.1 eV at very low excitation intensities due to local electric fields in these samples. From the analysis of the $I^{PL}(T)$, $\tau(T)$, and $I^{PL}(P_{\text{exc}})$ dependences for several samples, the electron- and hole-capture coefficients for the Ca_{Ga} acceptor are estimated as $C_n = (9 \pm 2) \times 10^{-14}$ cm³/s and $C_p = (6 \pm 2) \times 10^{-7}$ cm³/s, respectively.

From first-principles calculations using the HSE hybrid functional tuned to fulfill the generalized Koopmans condition, the −/0 transition level of the Ca_{Ga} acceptor is found at 0.70 eV above the VBM for the in-plane localized defect states (and 0.6 eV for the c -axis localized state), with the PL band maximum calculated at 2.23 eV (2.3 eV for the c -axis state). Although our theoretical results are somewhat closer to the experimentally found values than those previously reported in the literature [5,6], the reasons for the remaining disagreement are unclear. Parameters of the configuration coordinate model obtained from first-principles calculations and from the analysis of the experimental PL band shape are summarized in Table IV. In the latter case, Eqs. (5) and (6) were used, and it was assumed that $S_e/S_g = \hbar\Omega_e/\hbar\Omega_g$ [23].

Our experimental results agree with earlier findings. In particular, the 2.5-eV band with the shape and properties similar to the GL_{Ca} band was observed after implantation of GaN with Ca [7–9]. Chen and Skromme observed a green band with a maximum at 2.35 eV in Ca-implanted GaN [10]. This band is known as the GL2 band and is attributed to the isolated nitrogen vacancies [23]. The V_{N} and V_{N} -related complexes are often observed in implanted GaN [33,43]. A red band with a maximum at 1.8 eV observed by us (Fig. 1) and by Monteiro *et al.* [8] in Ca-implanted GaN is caused by the $V_{\text{N}}\text{Ca}_{\text{Ga}}$ complex [33]. A yellow band with a maximum at 2.2 eV [11] is most likely the C-related YL1 band due to contamination of GaN [2].

VI. CONCLUSION

The green (GL_{Ca}) band with a maximum at 2.5 eV in GaN is caused by electron transitions from shallow donors (at $T < 50$ K) or from the conduction band (at $T > 50$ K) to the −/0 level of the Ca_{Ga} acceptor located at 0.50 ± 0.02 eV above the valence band. The electron- and hole-capture coefficients for this defect are $C_n = (9 \pm 2) \times 10^{-14}$ cm³/s and

TABLE IV. The parameters of the configuration coordinate model.

Parameter	E_0 (eV)	$\hbar\omega_{\max}$ (eV)	S_e	S_g	$\hbar\Omega_e$ (meV)	$\hbar\Omega_g$ (meV)	d_{FC}^e (eV)	d_{FC}^g (eV)
Theory	2.80	2.23	13.5	16.6	28.2	34.4	0.38	0.57
Experiment	3.00 ± 0.02	2.50 ± 0.02	8.5 ± 1	10.5 ± 1.5	40 ± 5	50 ± 5	0.34 ± 0.08	0.53 ± 0.03

$C_p = (6 \pm 2) \times 10^{-7} \text{ cm}^3/\text{s}$, respectively, and they are independent of temperature. In undoped GaN grown at relatively low temperatures (600–800 °C), the contamination with Ca is responsible for the GL_{Ca} band, which was previously labeled the AL band [15,16]. The GL_{Ca} band can be detected in PL spectra when the concentration of Ca is as low as 10^{14} cm^{-3} due to the large hole-capture coefficient. The quantum efficiency of the GL_{Ca} band approaches unity in GaN implanted with high doses of Ca and annealed under ultrahigh nitrogen pressure. First-principles calculations predict the ionization energy and the PL band maximum at 0.7 and 2.23 eV, respectively.

ACKNOWLEDGMENTS

The work at VCU was supported by the National Science Foundation (Grant No. DMR-1904861) and by the VCU PeRQ Award. The calculations were performed at the VCU High Performance Research Computing (HPRC) Core Facility. The work at SUNY was supported by the National Science Foundation (Grant No. DMR-1905186). The work at IHPP was supported by Polish National Centre for Research and Development through Project No. TECHMATSTRATEG-III/0003/2019-00.

The authors declare no conflicts of interest.

- [1] H. Amano, Y. Baines, E. Beam, M. Borga, T. Bouchet, P. R. Chalker, M. Charles, K. J. Chen, N. Chowdhury, R. Chu *et al.*, The 2018 GaN power electronics roadmap, *J. Phys. D: Appl. Phys.* **51**, 163001 (2018).
- [2] M. A. Reshchikov, Measurement and analysis of photoluminescence in GaN, *J. Appl. Phys.* **129**, 121101 (2021).
- [3] M. A. Reshchikov and H. Morkoç, Luminescence properties of defects in GaN, *J. Appl. Phys.* **97**, 061301 (2005).
- [4] M. A. Reshchikov, J. D. McNamara, F. Zhang, M. Monavarian, A. Usikov, H. Helava, Yu. Makarov, and H. Morkoç, Zero-phonon line and fine structure of the yellow luminescence band in GaN, *Phys. Rev. B* **94**, 035201 (2016).
- [5] J.-X. Shen, D. Wickramaratne, C. E. Dreyer, A. Alkauskas, E. Young, J. S. Speck, and C. G. Van de Walle, Calcium as a non-radiative recombination center in InGaN, *Appl. Phys. Express* **10**, 021001 (2017).
- [6] J. L. Lyons, D. Wickramaratne, and C. G. Van de Walle, A first-principles understanding of point defects and impurities in GaN, *J. Appl. Phys.* **129**, 111101 (2021).
- [7] J. I. Pankove and J. A. Hutchby, Photoluminescence of ion-implanted GaN, *J. Appl. Phys.* **47**, 5387 (1976).
- [8] T. Monteiro, C. Boemare, M. J. Soares, E. Alves, and C. Liu, Green and red emission in Ca implanted GaN samples, *Physica B* **308-310**, 42 (2001).
- [9] E. Alves, C. Liu, E. B. Lopes, M. F. da Silva, J. C. Soares, C. Boemare, M. J. Soares, and T. Monteiro, Study of calcium implanted GaN, *Nucl. Instrum. Methods Phys. Res. B* **190**, 625 (2002).
- [10] L. Chen and B. J. Skromme, Spectroscopic characterization of ion-implanted GaN, in *GaN and Related Alloys – 2002*, edited by C. Wetzel, E. T. Yu, J. S. Speck, and Y. Arakawa, Mater. Res. Soc. Proc., Vol. 743 (Materials Research Society, 2003), pp. 755–760.
- [11] M. Godlewski, T. Suski, I. Grzegory, S. Porowski, J. P. Bergman, W. M. Chen, and B. Monemar, Mechanism of radiative recombination in acceptor-doped bulk GaN crystals, *Physica B* **273-274**, 39 (1999).
- [12] E. C. Young, N. Grandjean, T. E. Mates, and J. S. Speck, Calcium impurity as a source of non-radiative recombination in (In,Ga)N layers grown by molecular beam epitaxy, *Appl. Phys. Lett.* **109**, 212103 (2016).
- [13] C. Chèze, F. Feix, J. Lahnemann, T. Flissikowski, M. Krysko, P. Wolny, H. Turski, C. Skierbiszewski, and O. Brandt, Luminescent N-polar (In,Ga)N/GaN quantum wells achieved by plasma-assisted molecular beam epitaxy at temperatures exceeding 700 °C, *Appl. Phys. Lett.* **112**, 022102 (2018).
- [14] T. Auzelle, C. Sinito, J. Lahnemann, G. Gao, T. Flissikowski, A. Trampert, O. Brandt, and S. Fernández-Garrido, Interface Recombination in Ga- and N-Polar GaN/(Al,Ga)N Quantum Wells Grown by Molecular Beam Epitaxy, *Phys. Rev. Applied* **17**, 044030 (2022).
- [15] M. A. Reshchikov, F. Yun, D. Huang, L. He, H. Morkoç, S. S. Park, and K. Y. Lee, Photoluminescence of GaN grown by molecular beam epitaxy on freestanding GaN template, in *Materials and Devices for Optoelectronics and Microphotonics*, edited by R. B. Wehrspohn, R. Marz, S. Noda, and C. Soukoulis, Materials Research Society Symp. Proc., Vol. 722 (Materials Research Society, 2002), pp. 27–32.
- [16] M. A. Reshchikov, L. He, R. J. Molnar, S. S. Park, K. Y. Lee, and H. Morkoç, Aquamarine luminescence band in undoped GaN, in *GaN, AlN, InN and Their Alloys*, edited by C. Wetzel, B. Gill, M. Kuzuhara, and M. Manfra, Materials Research Society Symp. Proc., Vol. 831 (Materials Research Society, 2005), pp. 537–542.
- [17] K. Sierakowski, R. Jakiela, B. Lucznik, P. Kwiatkowski, M. Iwinska, M. Turek, H. Sakurai, T. Kachi, and M. Bockowski, High pressure processing of ion implanted GaN, *Electronics* **9**, 1380 (2020).
- [18] M. A. Reshchikov, Time-resolved photoluminescence from defects in GaN, *J. Appl. Phys.* **115**, 103503 (2014).

- [19] M. A. Reshchikov, M. Vorobiov, D. O. Demchenko, Ü. Özgür, H. Morkoç, A. Lesnik, M. P. Hoffmann, F. Hörich, A. Dadgar, and A. Strittmatter, Two charge states of the C_N acceptor in GaN: Evidence from photoluminescence, *Phys. Rev. B* **98**, 125207 (2018).
- [20] M. A. Reshchikov, M. A. Foussekis, J. D. McNamara, A. Behrends, A. Bakin, and A. Waag, Determination of the absolute internal quantum efficiency of photoluminescence in GaN co-doped with Zn and Si, *J. Appl. Phys.* **111**, 073106 (2012).
- [21] M. A. Reshchikov, A. A. Kvasov, M. F. Bishop, T. McMullen, A. Usikov, V. Soukhoveev, and V. A. Dmitriev, Tunable and abrupt thermal quenching of photoluminescence in high-resistivity Zn-doped GaN, *Phys. Rev. B* **84**, 075212 (2011).
- [22] M. A. Reshchikov, Temperature dependence of defect-related photoluminescence in III-V and II-VI semiconductors, *J. Appl. Phys.* **115**, 012010 (2014).
- [23] M. A. Reshchikov, D. O. Demchenko, J. D. McNamara, S. Fernández-Garrido, and R. Calarco, Green luminescence in Mg-doped GaN, *Phys. Rev. B* **90**, 035207 (2014).
- [24] M. A. Reshchikov, J. D. McNamara, M. Toporkov, V. Avrutin, H. Morkoç, A. Usikov, H. Helava, and Yu. Makarov, Determination of the electron-capture coefficients and the concentration of free electrons in GaN from photoluminescence, *Sci. Rep.* **6**, 37511 (2016).
- [25] J. F. Muth, J. H. Lee, I. K. Shmagin, and R. M. Kolbas, H. C. Casey Jr., B. P. Keller, U. K. Mishra, and S. P. DenBaars, Absorption coefficient, energy gap, exciton binding energy, and recombination lifetime of GaN obtained from transmission measurement, *Appl. Phys. Lett.* **71**, 2572 (1997).
- [26] J. Heyd, G. E. Scuseria, and M. Ernzerhof, Hybrid functionals based on a screened Coulomb potential, *J. Chem. Phys.* **118**, 8207 (2003).
- [27] D. O. Demchenko, I. C. Diallo, and M. A. Reshchikov, Magnesium acceptor in gallium nitride: II. Koopmans tuned HSE hybrid functional calculations of dual nature and optical properties, *Phys. Rev. B* **97**, 205205 (2018).
- [28] D. O. Demchenko, M. Vorobiov, O. Andrieiev, T. H. Myers, and M. A. Reshchikov, Shallow and Deep States of Beryllium Acceptor in GaN: Why Photoluminescence Experiments Do Not Reveal Small Polarons for Defects in Semiconductors, *Phys. Rev. Lett.* **126**, 027401 (2021).
- [29] D. O. Demchenko and M. A. Reshchikov, Koopmans' tuning of HSE hybrid density functional for calculations of defects in semiconductors: A case study of carbon acceptor in GaN, *J. Appl. Phys.* **127**, 155701 (2020).
- [30] D. O. Demchenko and M. A. Reshchikov, Blue luminescence and Zn acceptor in GaN, *Phys. Rev. B* **88**, 115204 (2013).
- [31] C. Freysoldt, J. Neugebauer, and C. G. Van de Walle, Fully *Ab Initio* Finite-Size Corrections for Charged-Defect Supercell Calculations, *Phys. Rev. Lett.* **102**, 016402 (2009).
- [32] C. Freysoldt, J. Neugebauer, and C. G. Van de Walle, Electrostatic interactions between charged defects in supercells, *Phys. Status Solidi B* **248**, 1067 (2011).
- [33] M. Vorobiov, O. Andrieiev, D. Demchenko, and M. A. Reshchikov (unpublished).
- [34] M. A. Reshchikov, Mechanisms of thermal quenching of defect-related luminescence in semiconductors, *Phys. Status Solidi A* **218**, 2000101 (2020).
- [35] M. A. Reshchikov, O. Andrieiev, M. Vorobiov, B. McEwen, F. Shahedipour-Sandvik, D. Ye, and D. O. Demchenko, Stability of the C_NH_i complex and the BL2 luminescence band in GaN, *Phys. Status Solidi B* **258**, 2100392 (2021).
- [36] M. Vorobiov, O. Andrieiev, D. O. Demchenko, and M. A. Reshchikov, Point defects in beryllium-doped GaN, *Phys. Rev. B* **104**, 245203 (2021).
- [37] R. Y. Korotkov, M. A. Reshchikov, and B. W. Wessels, Acceptors in undoped GaN studied by transient photoluminescence, *Physica B* **325**, 1 (2003).
- [38] M. A. Reshchikov, Giant shifts of photoluminescence bands in GaN, *J. Appl. Phys.* **127**, 055701 (2020).
- [39] D. C. Look and R. J. Molnar, Degenerate layer at GaN/sapphire interface: Influence on Hall-effect measurements, *Appl. Phys. Lett.* **70**, 3377 (1997).
- [40] M. A. Reshchikov, Point defects in GaN, in *Semiconductors and Semimetals: Defects in Semiconductors*, edited by C. Jagadish, V. Privitera, and L. Romano, Vol. 91 (Academic Press, Burlington, UK, 2015), pp. 315–367.
- [41] M. A. Reshchikov, A. Usikov, H. Helava, Yu. Makarov, V. Prozheeva, I. Makkonen, F. Tuomisto, J. H. Leach, and K. Uduary, Evaluation of the concentration of point defects in GaN, *Sci. Rep.* **7**, 9297 (2017).
- [42] Y. Y. Sun, T. A. Abteew, P. Zhang, and S. B. Zhang, Anisotropic polaron localization and spontaneous symmetry breaking: Comparison of cation-site acceptors in GaN and ZnO, *Phys. Rev. B* **90**, 165301 (2014).
- [43] M. A. Reshchikov, O. Andrieiev, M. Vorobiov, D. Ye, D. O. Demchenko, K. Sierakowski, M. Bockowski, B. McEwen, V. Meyers, and F. Shahedipour-Sandvik, Thermal annealing of GaN implanted with Be, *J. Appl. Phys.* **131**, 125704 (2022).